Materials Research Express

PAPER • **OPEN ACCESS**

Mechanical, and corrosive properties of AA7075 aluminium reinforced with rice husk ash particulates

To cite this article: O O Joseph *et al* 2023 *Mater. Res. Express* **10** 116520

Materials Research Express

PAPER

Mechanical, and corrosive properties of AA7075 aluminium reinforced with rice husk ash particulates

O O Joseph[1,*], J O Dirisu[1], J Atiba[1], S Ante[1] and J A Ajayi[2]

[1] Department of Mechanical Engineering, Covenant University, P.M.B 1023, Canaanland, Ota, Ogun State, Nigeria
[2] Department of Metallurgical & Materials Engineering, Federal University of Technology, P.M.B 704, Akure, Ondo State, Nigeria
* Author to whom any correspondence should be addressed.

E-mail: funmi.joseph@covenantuniversity.edu.ng **and** funmjoseph@gmail.com

Keywords: aluminium, rice husk ash, composite, reinforcement, metal matrix

OPEN ACCESS

RECEIVED
26 July 2023

REVISED
24 October 2023

ACCEPTED FOR PUBLICATION
17 November 2023

PUBLISHED
30 November 2023

Abstract

The mechanical and corrosive properties of AA7075 alloy reinforced with rice husk ash (RHA) particles were studied. AA7075 matrix composite reinforced with varying percentage weight compositions of rice husk ash particles (5%, 10%, 15% and 20% wt) were prepared using stir casting technique. The mechanical, and corrosive properties of the new material were compared with that of the matrix alloy. The mechanical properties were also improved due to the automated stirring action employed during the casting process. AA7075-RHA composites had improved mechanical properties compared to the base matrix (AA7075). In terms of tensile strength there was an increase in this mechanical property with an increase in weight fraction of RHA particle (51% at 10% RHA), hardness (25.67% at 20% RHA), while for impact resistance, the reverse was the case as there was a 10.98% decrease in the resistance of the composite as the reinforcement fraction increased from 0%–20% RHA. The progressive decreases in the impact strength of the reinforced composite were probably due to agglomeration and non-homogeneity at higher reinforcements values. Corrosion experiments carried out showed improved properties in the reinforced composite compared to the unreinforced alloy, the corrosive properties improved with an increase in weight fraction of RHA in terms of weight loss (20.63% at 10% RHA), potentio-dynamic polarization (30.7% at 10% RHA) and open circuit potential (1.60% at 20%RH). The developed composite may be suitably applied in high-speed rotating shafts and automotive engineered brake parts.

1. Introduction

The pace of innovation has resulted in an increasing demand for superior materials that have a good combination of various desirable properties. Strength, toughness, surface hardness, high corrosion resistance, ductility, good weldability, and machinability are all desirable properties while maintaining a lower weight than other materials. To meet this demand, various composite materials have been developed on a continuous basis [1, 2].

Aluminium matrix composites (AMCs) are a significant class of advanced technical materials in today's world. AMCs have a unique combination of characteristics that are sought after in a variety of industries and can replace traditional aluminium alloys in a variety of applications [3]. The cost of manufacturing AMCs is considerably high, which may limit their extensive use. One way to reduce production costs is to use industrial waste and natural minerals as reinforcing particles [4]. In comparison to traditional ceramic particles, rice husk ash (RHA) provides a cost-effective reinforcement. RHA is a type of agricultural waste that is abundant over the world. Rice, bran, and husk are the main components of milled paddy. This husk is used as fuel by rice mills to generate steam for the parboiling process. The volatile substance in the husk evaporates during the burning process, and the leftover husk is converted into RHA [5, 6].

Table 1. Chemical composition of AA 7075 alloy.

Element	Si	Cu	Fe	Zn	Mg	Ti	Ni	Pb
Wt%	9.89	2.09	0.53	0.79	0.15	0.053	0.086	0.030

Table 2. Chemical composition of RHA.

Element	SiO_2	Al_2O_3	Fe_2O_3	CaO	MgO	Na_2O	K_2O
Wt%	94.04	0.249	0.136	0.622	0.442	0.023	2.49

Common agricultural waste disposal practices involve techniques like depositing waste in undeveloped areas, along roadsides, or into water bodies. There are instances of open burning, and at times, the remains and their ashes are used as fertilizers. These conventional approaches result in the release of CO_2 through burning and disposal, while further contributing to the problem, methane and other gases are emitted as the agricultural waste decomposes [7, 8]. Rice husks poses a significant environmental risk, causing damage to the soil and the surrounding area where it is discharged. According to current research findings, RHA comprises approximately 85%−90% amorphous silica [9]. Thermal treatment turns silica to crystobalite, a crystalline form of silica. Amorphous silica with high reactivity, ultra-fine size, and enormous surface area is created under controlled burning circumstances. This micro silica can be used to make advanced materials such as SiC, Si_3N_4, elemental Si, and Mg_2Si [10].

This study is dedicated to the investigation of an innovative methodology involving the amalgamation of rice husk ash with aluminium to develop matrix composites utilizing the stir casting technique. Multiple weight ratios of rice husk particles are systematically explored. The primary objective of this research is to conduct a comprehensive assessment of the mechanical, electrochemical, and optical attributes of the resulting composites featuring rice husk ash. This effort is driven by the goal of mitigating environmental impact and optimizing cost-efficiency within the realm of advanced matrix composites (AMCs) through the development of a novel material characterized by superior performance properties.

2. Material and methods

2.1. Materials

Aluminium alloy 7075 (AA7075) was used as the matrix material. The chemical composition of the matrix material and the RHA particles was determined via x-ray flourescence (XRF). The chemical composition of the matrix material is given in table 1. RHA particulate with an average size of 300 μm was used as the reinforcement material. The chemical composition of RHA is given in table 2.

2.2. Composite preparation

Stir casting (with schematic shown in figure 1 was used to develop the aluminium metal matrix composite. A mechanical stirrer is used in the stir casting technique of manufacturing metals to uniformly mix the reinforcement that is introduced into the matrix material. This method was chosen for this study due to its distinct properties in terms of accessibility, simplicity, and affordability. A conventional stir casting system includes a mechanical stirrer, reinforcement particulate feeder, and furnace. The fundamental function of the furnace is to heat and melt the matrix materials prior to casting.

The samples were developed by altering the percentage by weight of reinforcement particles from 0 wt% to 20 wt% at 5 wt% intervals, with the balance being the base matrix (AA7075) following the specifications of ASTM B179 standard [11].

In total, 5 samples of different compositions were prepared. Table 3 shows the charge calculation for the metal matrix composite.

All the necessary equipment and materials were assembled, and all personal protective equipment was donned. The reinforcements and matrix were divided according to the mix design. Two patterns were prepared, A cylindrical pattern (200 mm long with a diameter of 20 mm) and cuboid (25 mm $\times$ 15 mm $\times$ 200 mm). Using the patterns prepared, 10 different mold samples were created: 5 cylindrical molds and 5 rectangle molds. The furnace was ignited, and the metal (base matrix) was introduced at 700 degrees into the oil-fueled tilting furnace. The reinforcement was then placed in the steel cup and fired at 700 °C for one minute. Molten metal was poured and mixed into the steel cup containing the fired forming a composite slurry which was stirred continuously for

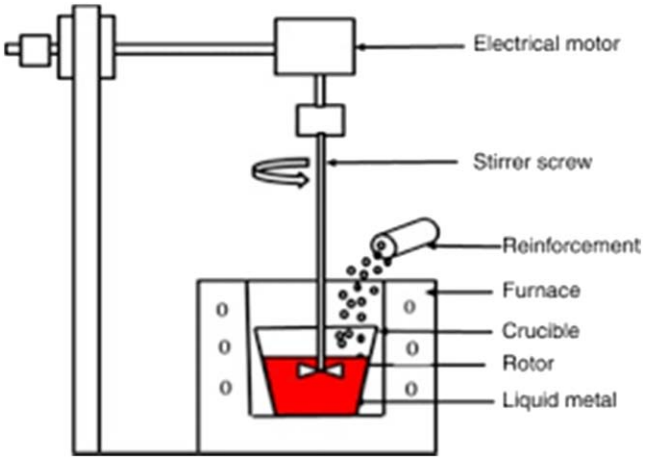

Figure 1. Schematic of stir casting technique. Reprinted from [12], Copyright (2015), with permission from Elsevier.

Table 3. Charge calculations for the AMCs.

S/NO	AA7075 Weight (g)	Weight of RHA (g)	Wt% of RHA
5% RHA	1000	52.63	2.5
10% MXT	1000	111.00	5.0
15% MXT	1000	176.47	7.5
20% MXT	1000	250	10.0
Control	1000	0	0

a period of 10 min at a speed of 400 rpm. The slurry was then poured into the hollow molds and allowed to solidify. This process was repeated for the four alternative material compositions and the control sample.

2.3. Microstructural analysis

The samples used for microstructural analysis were each machined to 15 × 15 × 5 mm. Sample surfaces for optical microscopy test were prepared particularly by grinding with various sizes of emery (silicon carbide) papers ranging from 150, 320, 400, 600, 800, and 1200 grits. Polishing cloth and alumina as a polishing paste were then used to polish the specimen. The samples were etched with sodium hydroxide after polishing, and the microstructure was viewed with an optical microscope at magnification of ×100.

2.4. Mechanical behaviour

2.4.1. Tensile test

At a predetermined grip separation, samples were inserted into the grips of a Universal Test Machine and pulled until failure occurs. The material specification or the time to failure can be used to calculate the ASTM D3039 test speed (1 to 10 min). A typical test speed for standard test specimens is 2 mm min^{-1} (0.05 in/min). An extensometer or strain gauge was used to quantify elongation and tensile modulus.

2.4.2. Hardness test

The Vickers hardness of the samples was determined using the Future Tech FV 800 Vickers hardness testing machine. Bakelite was used to keep the samples from shifting when the weight was applied. A diamond indenter was used to indent the material for 10 s at a force of 5 kg. To counterbalance the segregation impact of the matrix reinforcements, four measurements were taken for each sample.

2.4.3. Impact test

The impact test was carried out on the samples using the Charpy apparatus. The sample preparations and testing operations were carried out according to the procedures of [13].

2.5. Corrosive behaviour

2.5.1. Weight loss experiment

Each sample was machined to the required dimension of 20 mm × 20 mm × 10 mm for immersion test. The samples were weighed and immersed in a 0.5 M hydrochloric acid solution. Individual samples were then tagged and stored for the appropriate amount of time. After the total immersion period of 240 h had expired (weight loss readings were taken at 48 h intervals), the samples were removed from the test solution and washed with distilled water to eliminate corrosion deposits. Before weighing and recording the weight, the sample was allowed to dry.

The corrosion rate was calculated using the formula as follows [14–17]:

$$CR = \frac{W}{(D \times A \times t)} \times 87.6 \quad (1)$$

Where:

CR, W, D, A and t are the Corrosion Rate (mm/y), weight loss of the sample (mg), Metal density (2.7 g $cm^{-3)}$, cross-sectional Area (cm^2) and Exposure time (hours) of the sample.

2.5.2. Open circuit potential and potentiodynamic polarization test

Wires with an average length of 110 mm were soldered to the cylindrical aluminium matrix samples and mounted with acrylic resin (versoCit-2), which hardened in a matter of seconds. The mounted samples' surfaces were polished with several grades of abrasive paper up to 2000 microns. The potentiostat was connected to a computer system running the relevant software for analysis (DY2300EN). The working electrode was the mounted aluminium matrix samples, the reference electrode used was Ag/AgCl and the counter electrode was platinum wire. The polarization tests commenced with cathodic polarization at −1.50 V. A potential scan rate of 2 mV s^{-1} was used.

3. Results and discussion

3.1. Optical microstructure

Plate 1 shows the optical images of AA7075 aluminium with and without reinforcement at 100×. Image (a) shows the internal structure of the aluminium with no reinforcement. A bimodal size distribution of plate-shaped $\acute{\eta}$ variants can be seen [18]. Image (b) shows uniform distribution of the RHA particles across the aluminium (a darker image). Furthermore, this observation indicates a uniform distribution of RHA particles within the aluminium matrix, effectively occupying active sites for corrosion. This aligns with the empirical data presented in sections 3.6 and 3.7.

3.2. Tensile strength

From figures 2 and 3, aluminium-RHA of 10% wt. concentration had the highest tensile stress of 124 MPa. As the RHA weight concentration increased to 15% and 20% the tensile stress values (61.1246 MPa, 80.8870 MPa) reduced below the value of the control (82.4864 MPa). On an average the increase in concentration of RHA inclusion into the aluminium matrix tends to reduce the load the metal can withstand. Although from the results obtained, if rice husk is dispersed in AA7075 in the proportion of 10% wt. concentration, the aluminium matrix has the potential to withstand 51% more load as compared to the base material. A similar trend was observed in studies conducted by [7] and [19]. The rise in strength attributed to the reinforced particles is attributed to the diffusion influence of RH particulates within the aluminum matrix. This diffusion effectively obstructs micro-voids and gaps within aluminum's structure [20].

3.3. Hardness

Table 4 displays the Vickers hardness values of AMCs with varying weight percentages of rice husk reinforcements. The table shows that adding these particles to aluminum matrix composites improves their hardness when compared to unreinforced AMCs. Vickers hardness values range from unreinforced aluminum (99.48 HV) to AMC reinforced with 20% RHA (125.02 HV). Hardness values increase as reinforcement concentration increases; similar trends were observed in [21–23]. RHA particles in the aluminum matrix that are harder and better bonded prevent dislocations and increase the hardness of AMCs. Research indicates that robust intermetallic bonding between rice husk ash and aluminum contributes to material reinforcement [24]. However, it's not necessarily guaranteed that a greater addition of particulate reinforcements will lead to increased hardness. This is due to the limited availability of intermetallic ions for the particles to establish bonds with.

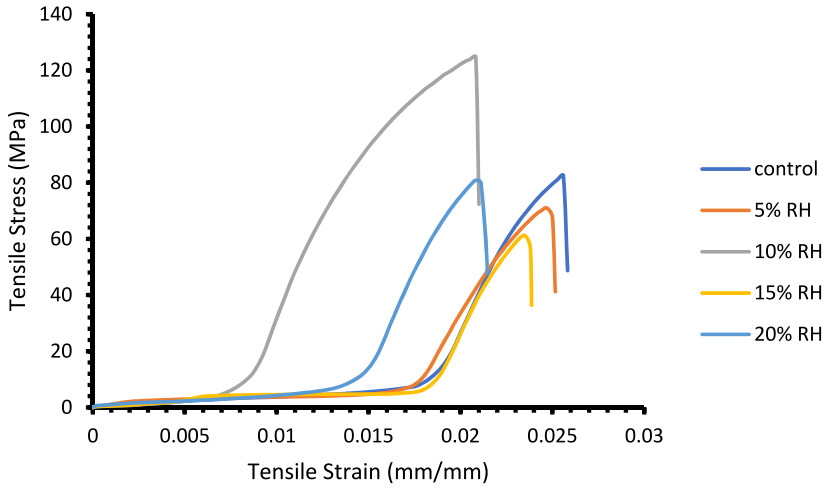

Figure 2. Tensile strength of RHA reinforced composites.

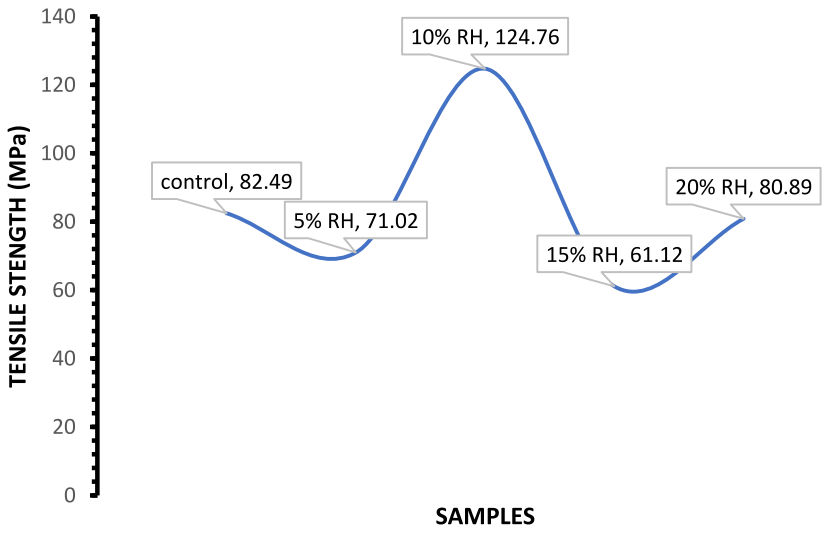

Figure 3. Tensile strength values against RHA samples.

Table 4. Vickers hardness of the composites.

Samples	Vickers hardness (HV)
Control (AA7075)	99.48
5% RHA	108.11
10% RHA	111.91
15% RHA	118.78
20% RHA	125.02

3.4. Impact resistance

The graphical representation in figure 4 shows the result of the impact resistance test performed on the RHA reinforced composites. The result showed a steady decline in the impact strength as the % wt. decreased except for the sample with 15%wt. RHA. This anomaly might stem from an uneven distribution of the reinforcement particles in the base matrix. The control sample had the highest impact resistance strength (12.02 J) while the composite with 20%wt RHA showed a 10.98% decrease and had the least impact resistance strength (10.70 J), this finding is in correlation with that of [18].

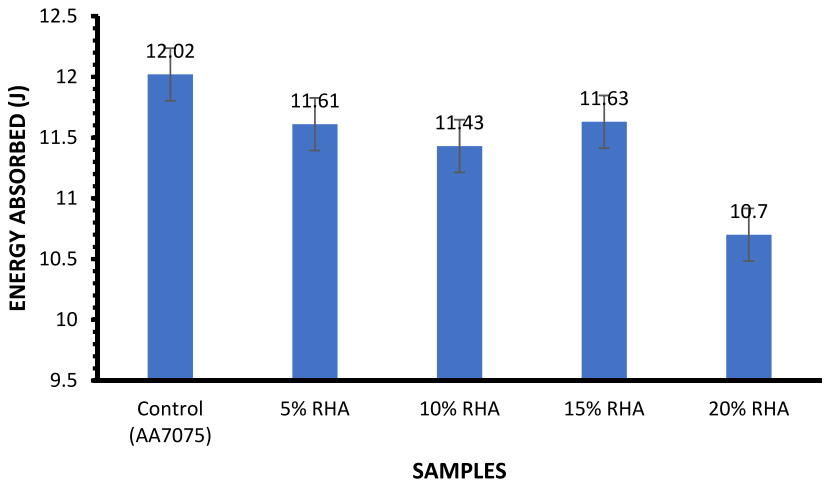

Figure 4. Impact resistance of aluminium-RHA reinforcements.

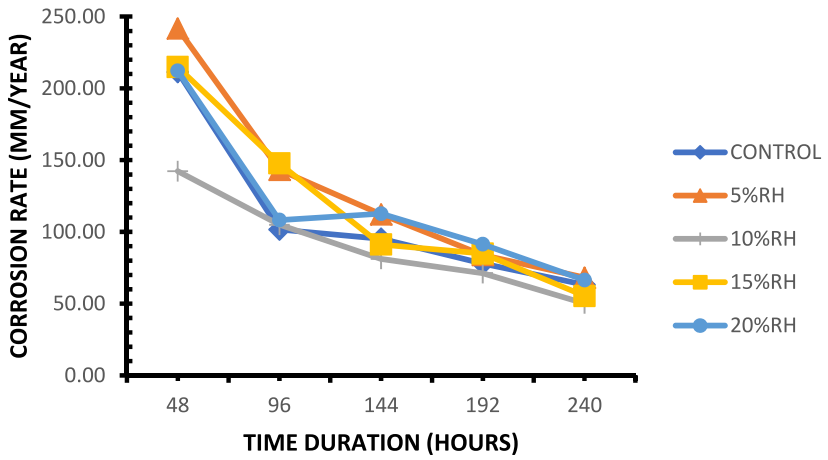

Figure 5. Corrosion rate of the Al-RHA composites.

3.5. Weight loss test

The graphical representation in figure 5 shows the changes in corrosion rate over time of different compositions of aluminium reinforced with rice husk when immersed in 0.5 M HCl acid environment. The control sample (AA7075) was also used in the analysis of the corrosion rate. From the result analysis, the corrosion rate of the samples in the HCl acid environment decreased over time. Although, at the end of the 240 h period, the Aluminium with 10% in composition of rice husk showed the least corrosion rate while the Aluminium with 5% in composition of rice husk showed the highest corrosion rate at the same period [25]. The presence of the fibre reinforcements migrating towards the active sites of the base metals acts as an inhibitive agent preventing the attack of chloride ions on the surface of aluminium [26].

3.6. Open circuit potential plots

Figure 6 shows the open circuit potential (OCP) curves of Aluminium-PKS and the control sample in 0.5 M HCl. The aluminium with 5 wt% PKS concentration started with a potential value of −0.696 v and gradually decreased to around −0.696 v after 100 s. After 100 s, the potential value began to rise, eventually reaching −0.676 v after 600 s. After 600 s, the aluminium with 10 wt% PKS concentration had a positive potential value rise from −0.704 v to −0.686 v. Aluminium with 15 wt% PKS concentration produced an overall slow increase with starting and ending potential values of −0.692 v and −0.688 v, respectively. The figure above shows a steady electropositive potential increase with the 20 wt% concentration, with the potential value increasing from −0.682 v to −0.662 v between the 100 s and 600 s time frame. The composition with the least potential value has the least tendency to corrode, and as shown in figure 5, the aluminium with 20 wt% PKS concentration has the least potential value, implying that it corroded least amongst all the samples. The plot's placement indicates the

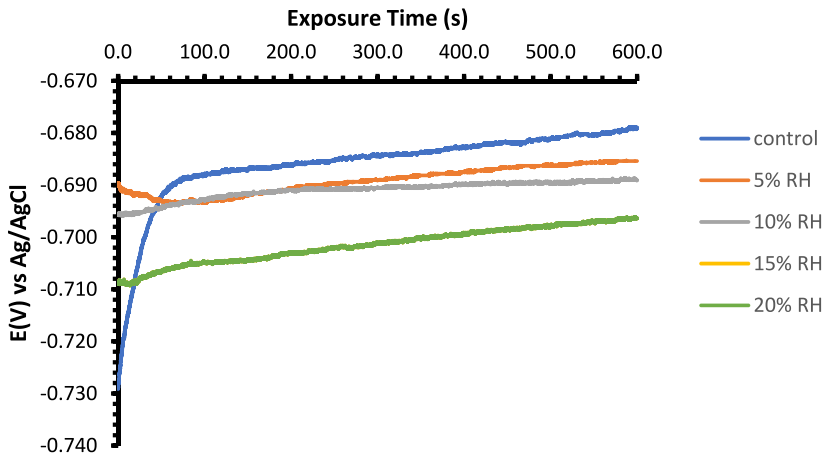

Figure 6. OCP plots of aluminium-RHA reinforcements.

Table 5. Potentiodynamic polarization results for Al-RHA reinforcements and the control sample in 0.5 M HCl.

Sample	C_R (mm/yr)	C_p(V)	C_d (A/cm^2)	R_P (Ω)	B_a (v/dec)	B_c (V/dec)
control	2.300	−0.698	1.98E-04	129.40	12.080	−6.822
5% RHA	1.592	−0.725	1.37E-04	187.10	18.350	−6.868
10% RHA	1.987	−0.728	1.71E-04	149.90	15.870	−6.841
15% RHA	2.221	−0.765	1.92E-04	134.10	10.200	−8.368
20% RHA	2.290	−0.724	2.53E-04	101.30	16.300	−6.627

prevailing intensity of the cathodic reaction relative to the anodic reaction within the system. This positioning underscores the cathodic nature of reinforcement exhibited by RHA. This nature of reinforcement can be attributed to the pronounced prominence of cathodic behaviour within the system's electrochemical response [27, 28].

3.7. Potentio-dynamic polarization test

Table 5 shows the polarization test results in terms of corrosion rate (CR), corrosion current density (Cd), corrosion potential (Cp), polarization resistance (Rp), and anodic and cathodic Tafel slope. The control sample corroded rapidly in the presence of Cl- ions, with a corrosion rate of 2.300 mm yr^{-1}., whereas the aluminium with 5 wt% RHA concentration had the lowest corrosion rate of 1.592 mm yr^{-1}. Because its particles were more evenly distributed within the matrix than the other RHA reinforcements, the 5 wt% RHA concentration had the lowest corrosion rate [29, 30]. The disparities in corrosion rates within the composite could also be attributed to the presence of physio-chemical heterogeneous factors, including defects, mechanically compromised surfaces, dislocations, and intermetallic or alloy/reinforcement interfaces. Another study also highlights that the elevated corrosion rate linked with higher composition of RHA may arise from the larger volume of RHA particulates with a lower density (0.3 g cm^{-3}) compared to AA7075 (2.7 g cm^{-3}), resulting in an increased vulnerability of numerous alloy/reinforcement interfaces to corrosion [12], usually caused by trapped Cl^- ions within the intermetallic surface.

The current density values increased as RHA concentration increased from 1.98E-04 to 2.53E-04 A cm^{-2}. The anodic Tafel slope value also increased from 12.080 V dec^{-1} to 16.300 V dec^{-1}, and as a result, an increase in anodic current density triggers metal dissolution processes on the aluminium surface. The aluminium with the highest polarization resistance of 134.10 was obtained with a 15% RHA wt. concentration, similar observation were made in the research of [31, 32]. The polarization plot of AL-RHA reinforcements and the control sample at 0.5 M HCl is shown in figure 7.

4. Conclusion and recommendations

4.1. Conclusions

The following conclusions can be made from the foregoing analysis of this research:

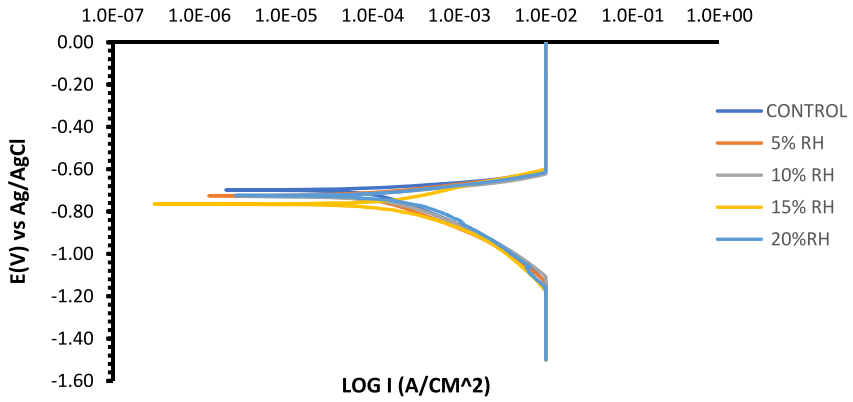

Figure 7. Potentiodynamic polarization plot for AL-RHA composites.

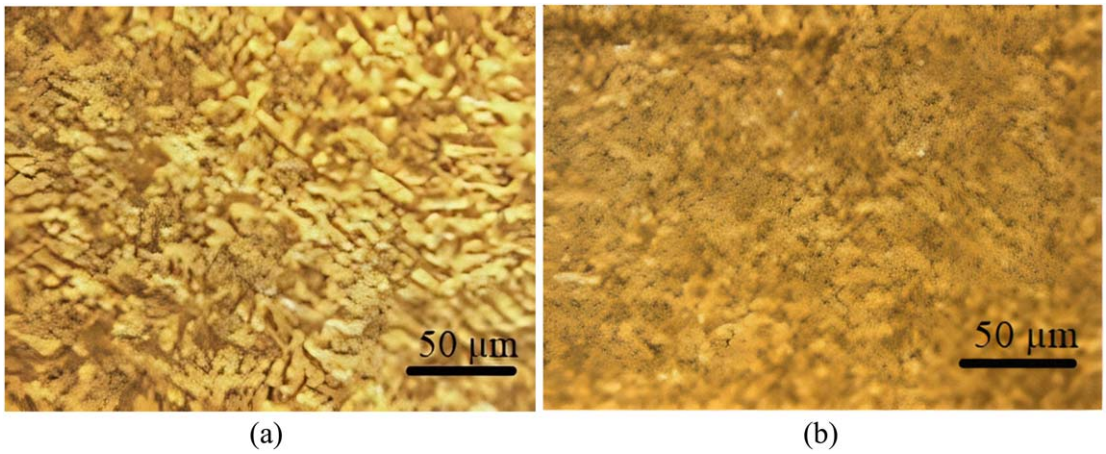

Plate 1. Microstructure of (a) AA7075 aluminum without reinforcement and (b) AA7075 aluminum composite reinforced RHA particles.

i. The mechanical properties of the reinforced AA7075 significantly improved compared to the unreinforced AA7075 alloy.

ii. The tensile strength, hardness of the reinforced AA7075-RH increased with an increase in percentage weight charge of rice husk ash. The optimum increase point for the tensile strength and hardness were 10 wt% RHA and 20 wt% RHA, respectively.

iii. The impact strength of the composites reduced with increase in percentage weight fraction of RHA due to agglomeration of the RHA within the primary phase of AA7075 matrix. The optimum value was observed at the control sample (AA7075)

iv. The corrosion rate reduced in all the reinforced samples when compared to that of the control samples.

Based on the research, RHA as a reinforcing material has demonstrated promising potential. This could aid in mitigating the adverse environmental effects caused by agro-waste within our community, while also contributing to a reduction in the procurement cost of aluminium matrix composites.

4.2. Recommendations

To unlock the full potential of rice husk ash (RHA) as a reinforcing material, it is advisable to embark on further research with the goal of optimizing the appropriate RHA content within aluminium alloys. Achieving an optimal equilibrium between mechanical properties, impact resistance, and corrosion resistance is paramount when tailoring materials for specific applications. Additionally, broadening the research scope to encompass a wider array of agricultural and industrial waste materials for potential reinforcement in diverse alloy systems offers a promising avenue for both sustainable material development and the efficient utilization of waste. It is

strongly recommended that RHA-reinforced materials undergo real-world testing in applications such as high-speed rotating shafts and automotive braking components.

Acknowledgments

Covenant university is gratefully acknowledged for open access funding.

Data availability statement

All data that support the findings of this study are included within the article (and any supplementary files).

ORCID iDs

O O Joseph https://orcid.org/0000-0002-7088-8055
J Atiba https://orcid.org/0009-0006-8644-5909

References

[1] Alaneme K K, Ekperusi J O and Oke S R 2018 Corrosion behaviour of thermal cycled aluminium hybrid composites reinforced with rice husk ash and silicon carbide *J. King Saud Univ. - Eng. Sci.* **30** 391–7
[2] Thirumoorthy A, Arjunan T V and Senthil Kumar K L 2018 Latest research development in aluminum matrix with particulate reinforcement composites - a review *Mater. Today Proc.* **5** 1657–65
[3] Knowles A J, Jiang X, Galano M and Audebert F 2015 Microstructure and mechanical properties of 6061 Al alloy based composites with SiC nanoparticles *J. Alloys Compd.* **615** S401–5
[4] Narasimha Murthy I, Venkata Rao D and Babu Rao J 2012 Microstructure and mechanical properties of aluminum-fly ash nano composites made by ultrasonic method *Mater. Des.* **35** 55–65
[5] Soltani N, Bahrami A and González L A 2014 Review on the physicochemical treatments of rice husk for productionof advanced materials *Chem. Eng. J.* **264** 899–935
[6] Dinaharan I, Kalaiselvan K and Murugan N 2017 Influence of rice husk ash particles on microstructure and tensile behavior of AA6061 aluminum matrix composites produced using friction stir processing *Compos. Commun.* **3** 42–6
[7] Usman A M, Raji A, Waziri N H and Hassan M A 2014 Aluminium alloy - rice husk ash composites production and analysis, *Leonardo Electron. J. Pract. Technol.* **13** 84–98
[8] Joseph O O and Babaremu K O 2019 Agricultural waste as a reinforcement particulate for aluminum metal matrix composite (AMMCs): a review *Fibers* **7** 33
[9] Gupta V K, Gupta M and Sharma S 2001 Process development for the removal of lead and chromium from aqueous solutions using red mud - An aluminium industry waste *Water Res.* **35** 1125–34
[10] Saravanan S D and Kumar M S 2013 Effect of mechanical properties on rice husk ash reinforced aluminum alloy (AlSi10Mg) matrix composites *Procedia Eng.* **64** 1505–13
[11] Senthilkumar T and Venkatesh S 2016 R. K.-J. of chemical, and undefined 2016 Evaluation of mechanical properties of Al-6082 based hybrid metal matrix composite *Researchgate.Net* **8** 58–64 (https://researchgate.net/profile/Ts-Senthilkumar/publication/306182553_Evaluation_of_mechanical_properties_of_Al-6082_based_hybrid_metal_matrix_composite/links/604b7d94299bf13c4fff62fb/Evaluation-of-mechanical-properties-of-Al-6082-based-hybrid-metal)
[12] Thandalam S K, Ramanathan S and Sundarrajan S 2015 Synthesis, microstructural and mechanical properties of *ex situ* zircon particles (ZrSiO4) reinforced metal matrix composites (MMCs): a review *J. Mater. Res. Technol.* **4** 333–47
[13] IS, IS 1757 1998 Method for charpy impact test (V notch) for metallic material [Online]. Available: https://archive.org/details/gov.in.is.1757.1988
[14] Loto R T 2022 Investigation of the protection effect of ginger, tea tree and grapefruit essential oil extracts on mild steel in 0.5 M H2SO4 solution *Mater. Res. Express* **9** 066509
[15] Omotosho O A, Okeniyi J O and Ikotun J O 2018 Corrosion behaviour of mild steel in 0.5 M sulphuric acid *Journal of Engineering and Applied Sciences* **13** 5789–95
[16] Okeniyi J O, Ikotun J O, Akinlabi E T and Okeniyi E T 2019 Anticorrosion behaviour of Rhizophora mangle L. bark-extract on concrete steel-rebar in saline/marine simulating-environment *The Scientific World Journal* **2019** 6894714
[17] Joseph O O, Fayomi O S I, Joseph O O, Afolalu S A, Mubaiyi M P, Olotu O N and Fashola J O 2022 A comparative study on the corrosion behaviour of welded and un-welded API 5L X70 steel in simulated fuel grade ethanol.' *Cogent Engineering* **9** 2009091
[18] Park J K and Ardell A J 1983 Microstructures of the commercial 7075 Al alloy in the T651 and T7 tempers *Met. Trans. A* **14** 1957–65
[19] Rao D M and Bandam B R 2014 Preparation and characterization of AL-Fly Ash metal matrix composite by stir casting method *Int. J. Innov. Sci. Mod. Eng.* **3** 1–5
[20] Udoye N E, Nnamba O J, Fayomi O S I, Inegbenebor A O and Jolayemi K J 2020 Analysis on mechanical properties of AA6061/Rice husk ash composites produced through stir casting technique *Mater. Today Proc.* **43** 1415–20
[21] Senthilkumar M, Saravanan S D and Shankar S 2014 Dry sliding wear and friction behavior of aluminum–rice husk ash composite using Taguchi's technique, *J. Compos. Mater.* **49** 2241–50
[22] Masuda T, Sauvage X, Hirosawa S and Horita Z 2020 Achieving highly strengthened Al–Cu–Mg alloy by grain refinement and grain boundary segregation *Mater. Sci. Eng.* A **793** 139668
[23] Khatekar N V and Pawade R S 2019 Analysis and modeling of surface characteristics in electrophoretic deposition–assisted internal polishing of AISI 304 steel *Int. J. Adv. Manuf. Technol.* **104** 3083–94
[24] Fayomi J, Popoola A P I, Oladijo O P, Popoola O M and Fayomi O S I 2019 Experimental study of ZrB2-Si3N4 on the microstructure, mechanical and electrical properties of high grade AA8011 metal matrix composites *J. Alloys Compd.* **790** 610–5

[25] Dwivedi S P, Sharma P and Saxena A 2020 Utilization of waste spent alumina catalyst and agro-waste rice husk ash as reinforcement materials with scrap aluminium alloy wheel matrix *Proc. Inst. Mech. Eng. Part E J. Process Mech. Eng.* **234** 543–52
[26] Kanayo Alaneme K and Apata Olubambi P 2013 Corrosion and wear behaviour of rice husk ash - Alumina reinforced Al-Mg-Si alloy matrix hybrid composites *J. Mater. Res. Technol.* **2** 188–94
[27] Zhang X *et al* 2019 Study on microstructure and tensile properties of high nitrogen Cr-Mn steel processed by CMT wire and arc additive manufacturing *Mater. Des.* **166** 107611
[28] Duraibabu D, Alagar M and Kumar S A 2014 Studies on mechanical, thermal and dynamic mechanical properties of functionalized nanoalumina reinforced sulphone ether linked tetraglycidyl epoxy nanocomposites *RSC Adv.* **4** 40132–40
[29] Lysenko V I, Gaponov S A, Smorodsky B V, Yermolaev Y G, Kosinov A D and Semionov N V 2016 Influence of coating permeability and roughness on supersonic boundary layer stability *AIP Conf. Proc.* 1770
[30] Wang X, Lee E, Xu C and Liu J 2021 High-efficiency, air-stable manganese–iron oxide nanoparticle-pigmented solar selective absorber coatings toward concentrating solar power systems operating at 750 °C *Mater. Today Energy* **19** 100609
[31] Alaneme K K, Adewale T M and Olubambi P A 2014 Corrosion and wear behaviour of Al-Mg-Si alloy matrix hybrid composites reinforced with rice husk ash and silicon carbide *J. Mater. Res. Technol.* **3** 9–16
[32] Fayomi O S I, Akande I G, Popoola A P I, Popoola S I and Daramola D 2019 Structural characterization and corrosion properties of electroless processed Ni[sbnd]P[sbnd]MnO2 composite coatings on SAE 1015 steel for advanced applications *J. Sci. Adv. Mater. Devices* **4** 285–9